Superconductor Science and Technology

PAPER

Effect of carbon doping on magnetic flux pinning and superconducting performance in $FeSe_{0.5}Te_{0.5}$ single crystals

To cite this article: J Zhang *et al* 2023 *Supercond. Sci. Technol.* **36** 025008

IOP Publishing Superconductor Science and Technology
Supercond. Sci. Technol. **36** (2023) 025008 (9pp) https://doi.org/10.1088/1361-6668/acadb5

Effect of carbon doping on magnetic flux pinning and superconducting performance in $FeSe_{0.5}Te_{0.5}$ single crystals

J Zhang[1,2], Jens Hänisch[2], X S Yang[1,*], K Zhao[1] and Y Zhao[1,3,4,*]

[1] Superconductivity and New Energy R&D Center, School of Physical Science and Technology, Southwest Jiaotong University, Chengdu 610031, People's Republic of China
[2] Institute for Technical Physics, Karlsruhe Institute of Technology, Hermann-von-Helmholtz-Platz 1, Eggenstein-Leopoldshafen 76344, Germany
[3] College of Physics and Energy, Fujian Normal University, Fuzhou 350117, People's Republic of China
[4] Fujian Provincial Collaborative Innovation Center for Advanced High-Field Superconducting Materials and Engineering, Fujian Normal University, Fuzhou 350117, People's Republic of China

E-mail: xsyang@swjtu.edu.cn and zhaoyong@fjnu.edu.cn

Received 18 September 2022, revised 12 December 2022
Accepted for publication 21 December 2022
Published 11 January 2023

Abstract

A series of carbon-doped single crystals with nominal composition $FeSe_{0.5}Te_{0.5}$ were synthesized by a self-flux method. X-ray diffraction indicated that the lattice parameter c increases with increasing carbon content, suggesting that carbon atoms enter the lattice. The critical current densities were measured and the flux pinning mechanism and its change with doping were analyzed. These samples showed a higher J_c in high magnetic fields as well as a narrower superconducting transition. We studied the impact of the introduction of carbon into $FeSe_{0.5}Te_{0.5}$ on the temperature dependence of the irreversibility field $H_{irr}(T)$ and upper critical field (H_{c2}). The pinning mechanism for the system was obtained via analysis of J_c.

Keywords: $FeSe_{0.5}Te_{0.5}$, critical current density, superconductivity, carbon

(Some figures may appear in colour only in the online journal)

1. Introduction

Iron-based superconductors (IBSs) are recognized as one of the main classes of superconducting materials and possess immense potential. They introduce profound variation to the field of electric power and high-field magnet technology [1]. Among the IBSs, FeSe, which has the simple tetragonal structure of PbO-type compounds and belongs to the specific '11' system, has been intensively studied [2]. Various methods can be used to improve the superconducting transition temperature, T_c, which can be an increased from 9 K to 40 K, for example monolayer film engineering, carrier doping and intercalation [3]. Substitution of Se by Te shrinks the lattice cell of FeSe, resulting in negative chemical pressure [4]. To easily control the electronic state, chemical modulation has the advantage of ambient pressure operation compared with the above-mentioned techniques.

Partial substitution of Se by Te can lead to a higher T_c of ∼14 K compared with FeSe (∼9 K) [5]. The simple structure and somewhat lower toxicity of Fe(Se,Te) compared with pnictide IBSs mean that these superconductors have had much research attention [6]. Due to the square planar lattice of Fe with tetrahedral coordination with Se/Te atoms and Fermi

* Authors to whom any correspondence should be addressed.

surface topology [7], the Fermi surface around the zero-energy bound states and higher-energy discrete states is likely to be related to the superconducting mechanism.

According to previous reports [8], the atoms in 3d metal series that replace Fe in $FeTe_{0.5}Se_{0.5}$ can significantly affect the superconducting properties. Structurally, this compound consists of buckled Fe(Se/Te) layers stacked along the *c*-axis. The electronic states in $FeSe_{0.5}Te_{0.5}$ derive from hybridization between Fe 3d and Te 5p (Se 4p) orbitals and have a complex dependence on average composition. Although various elements such as Cr, Mn, Ni, Cu and Ag have been studied as Fe dopants and proved to be able to induce superconductivity [9–14], there is a lack of research on light element doping compared with metal element doping.

Carbon substitution and its effect on critical current density (J_c) and upper critical field (H_{c2}) has been widely studied in MgB_2, and improvement of J_c at elevated fields has been shown [15]. Carbon in the MgB_2 system can enhance the lattice distortion of boron atoms and the internal stress of the crystal lattice, thereby enhancing electron scattering within the crystal lattice and increasing H_{c2}. In our work, by analyzing magnetization properties based on the critical state mode, we investigate the influence of doped C in $FeSe_{0.5}Te_{0.5}$ single crystal on the pinning mechanism.

To our knowledge, C doping of $FeSe_{0.5}Te_{0.5}$ or any chalcogenide IBS single crystal has not yet been reported. In this work, C-$FeSe_{0.5}Te_{0.5}$ single crystals were obtained through the self-flux method by introducing graphite. Our results indicate that the introduction of C into the crystal increases the lattice constant *c*, thereby weakening the layer coupling via van der Waals forces and enhancing the critical current density in high magnetic fields. Our results provide a simple and effective way to improve the flux pinning properties and achieve higher critical current densities in Fe(Se,Te) superconductors in high magnetic fields through non-metal doping.

2. Experimental methods

High-purity elemental Fe (99.99%), Se (99.999%), Te (99.999%) and graphite (99%) powders were purchased from Sigma Aldrich. These raw materials were then weighed and mixed in the stoichiometric molar ratio Fe:Se:Te:C $= 1 - x$:0.5:0.5:x ($x = 0$, 0.03, 0.07, 0.1) in a glove box in order to obtain a homogeneous reagent. Then, under a uniaxial pressure of 8 MPa, the mixed powders were pressed into pellets with a diameter of 10 mm and a thickness of 1 mm. Subsequently, these pellets were sealed in evacuated quartz tubes. Finally, the assemblies were heated up to 1085 °C, held for 36 h, then cooled at 5 °C h^{-1} to 400 °C and finally oven-cooled for 24 h to room temperature. The samples obtained were named according to the amount of C: undoped, 0.03 C, 0.07 C and 0.1 C.

The crystallinity of the samples was determined by x-ray diffraction (XRD; $\lambda = 1.5418$ Å, θ–2θ scans over 10–70°) on an X'Pert PANalytical XRD system at room temperature. Surface morphology was observed by a field-emission scanning electron microscope (JSM-7800F). Magnetization was measured with a SQUID magnetometer (MPMS, Quantum Design) under DC mode in zero-field-cooling and field-cooling. Electrical transport was measured down to 4.2 K and in magnetic fields perpendicular to the large surface up to 9 T with $H//c$. The standard four-probe method was used for resistivity measurements in a physical properties measurement system (Quantum Design).

3. Results and discussion

Figures 1(a) and (b) illustrate the typical size and lamellar morphology of the single crystals. The XRD patterns of all samples are compared in figure 1(c). All the main peaks belong to tetragonal P4/*nmm*, indicating that C doping does not alter the crystal structure. Moreover, all the major diffraction peaks of these samples come from (0 0 *l*) planes, indicating that the samples have a uniform *c*-axial orientation. The full width at half-maximum of all prominent diffraction peaks is less than 0.07°, revealing that the samples are crystallized and highly *c*-axis oriented. The relationship between the lattice parameters *c* and the C concentration is shown in figure 1(d). With the introduction of elemental C the lattice constant *c* is obviously increased. This may be mainly due to the fact that the ionic radius of C influences the unit cell dimension of $FeTe_{0.5}Se_{0.5}$. As the increase in lattice constant *c* shows, graphite doping leads to an expansion of the unit cell, indicating that the C atoms are incorporated into the $FeTe_{0.5}Se_{0.5}$ crystal structure. Qualitatively, the doped samples are much more easily cleaved than the undoped sample, which indicates a certain weakening of the van der Waals forces between the Fe-chalcogenide layers. Therefore, we assume that the position of the C atoms is interstitial between the layers.

As shown in figures 2(a) and (b), all samples have a sharp superconducting transition in the $M(T)$ curves. T_c decreases roughly linearly with C content *x,* with a slope of $dT_c/dx = -0.0374$ K/%. This is in contrast to C doping of FeSe single crystals [16], where T_c increases for similar doping levels. Hence, the presumably interlayer C doping in $FeSe_{0.5}Te_{0.5}$ has a similar, but much smaller, effect to excess Fe [17] and transition metal (Co, Ni, Cu) doping on the Fe site [9, 10, 18]. Despite the slight reduction in T_c, the superconducting volume fraction and/or the phase homogeneity are increased by C doping, as the increase in magnetization (figure 2(a)) as well as in the XRD signal (figure 1(c)) show.

Figure 3 shows the magnetization hysteresis loops of all the samples measured from −6 T to 6 T at 6 K, 8 K and 10 K and for $H//c$. It shows typical superconductor isothermal magnetization hysteresis loops $M(H)$, whose area is found to steadily shrink with increasing temperature due to the weakening of pinning by the higher temperature. All $M(H)$ loops are rather symmetric with respect to the field direction, implying that bulk pinning dominates magnetization

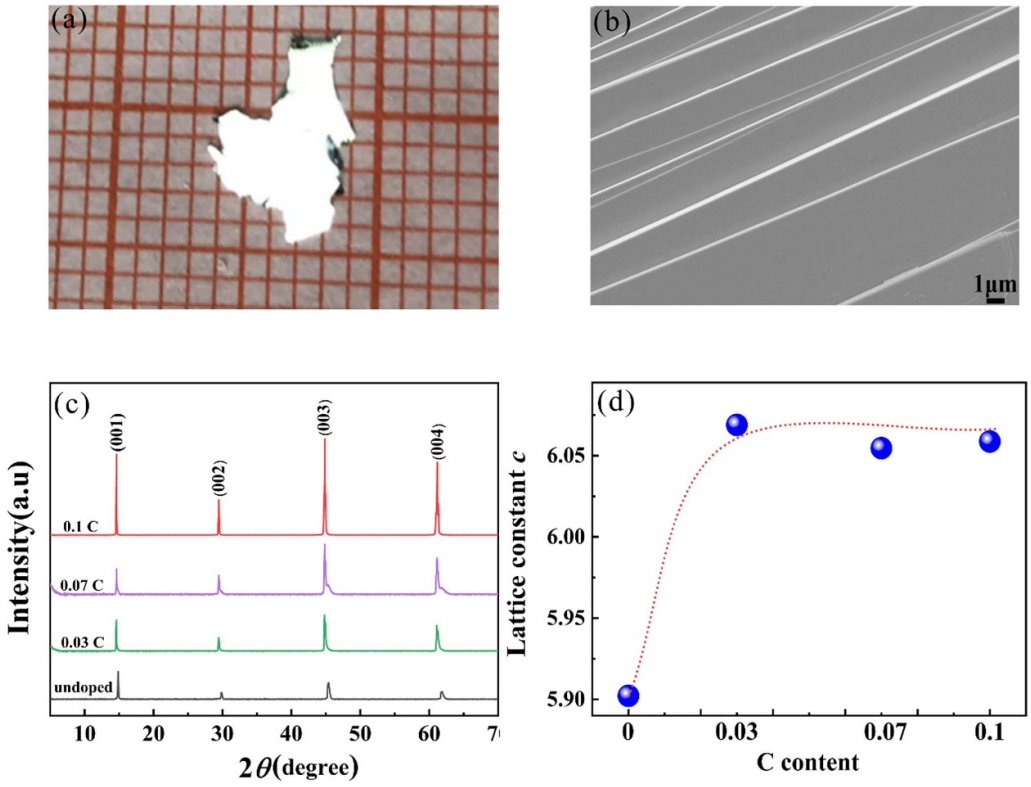

Figure 1. (a) Photograph of the 0.1 C single crystal. (b) Scanning electron microscope images of the 0.1 C single crystal. (c) XRD patterns of all samples with different C contents. (d) Lattice parameter c versus C concentration.

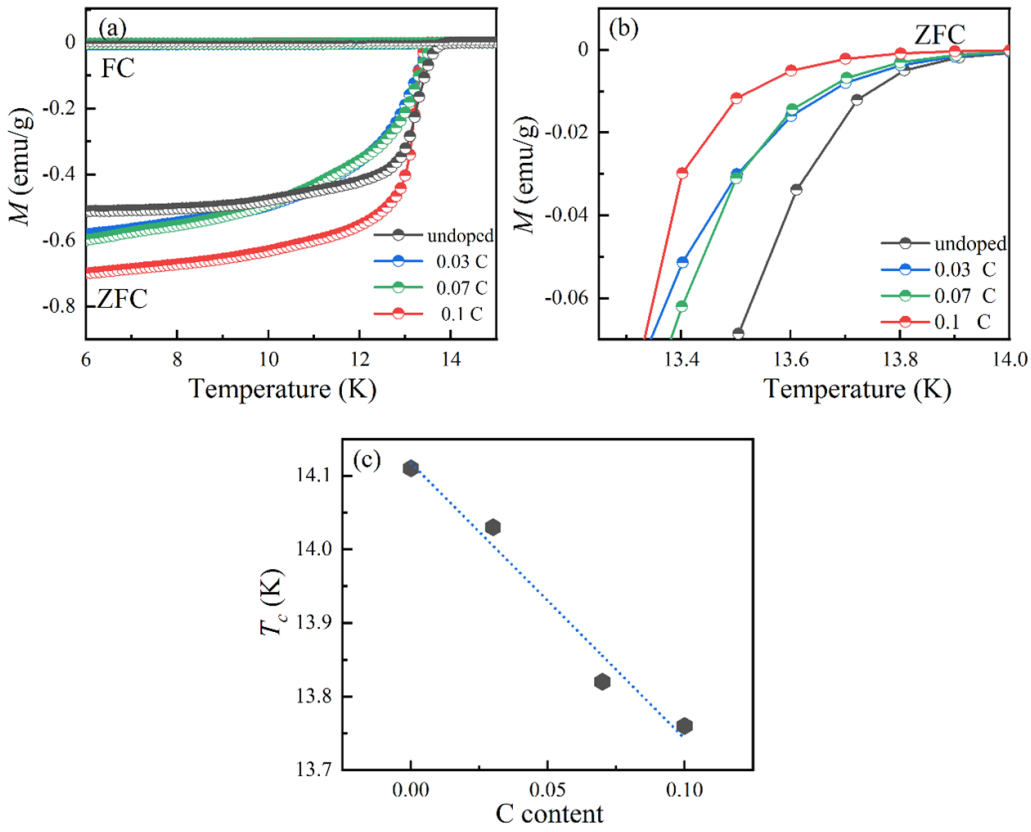

Figure 2. (a) $M(T)$ curves and (b) enlarged $M(T)$ curves of the samples. (c) T_c as a function of C doping level for all the single-crystal samples.

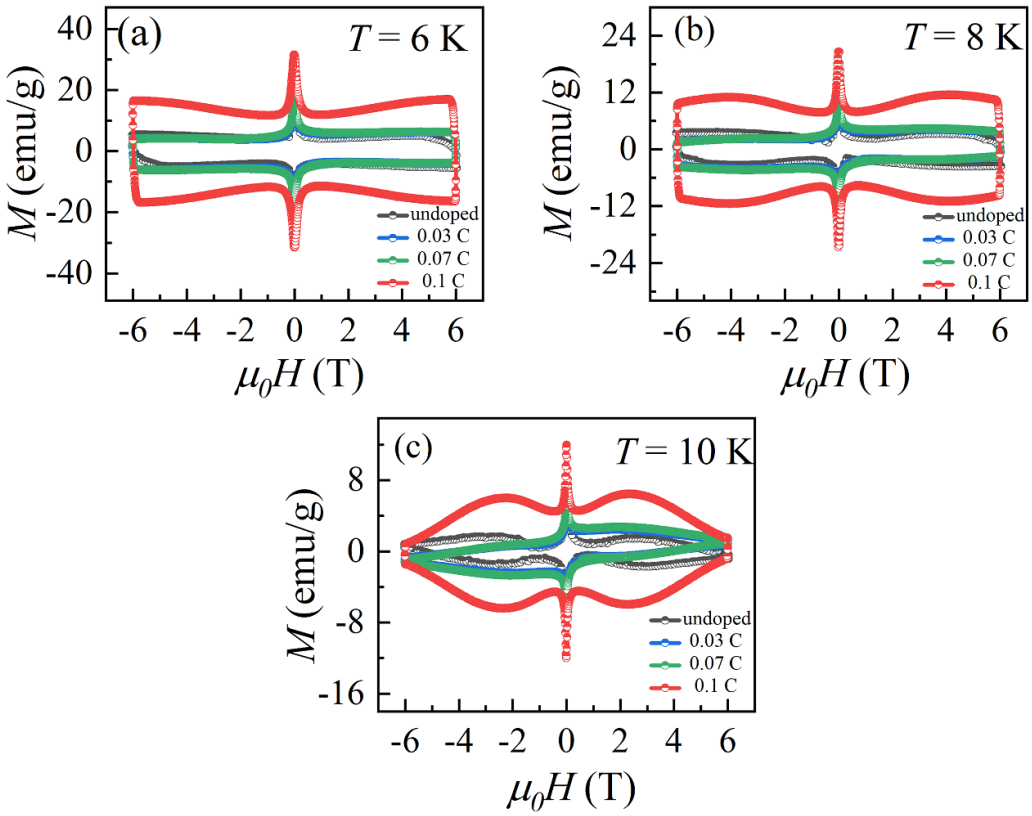

Figure 3. The magnetization hysteresis loops of all the single-crystal samples measured at (a) 6 K, (b) 8 K and (c) 10 K.

hysteresis in this compound. The presence of a second magnetization peak (SMP) is clearly visible and detectable up to 10 K in the undoped and 0.1 C samples (figure 3). Similar results were reported for $YBa_2Cu_3O_{7-\delta}$ crystals [18–20] and other Fe-based superconductors [20–23] for different kinds of doping.

From the $M(H)$ loops of figures 3(a)–(c), the critical current densities $J_c(H)$ in figures 4(a)–(c) were calculated using the Bean critical state model [24]

$$J_c = 20\frac{\Delta M}{a\left(1-\frac{a}{3b}\right)} \quad (1)$$

where $\Delta M = M_- - M_+$, M_- and M_+ are the magnetizations measured with decreasing and increasing fields, respectively, and a and b ($b > a$) are the sizes of the rectangular crystal perpendicular to the applied field. For $J_c(H)$ curves at $T = 6$ K and $T = 8$ K, the critical current density decreases at first, then roughly stabilizes, while the $J_c(H)$ curves at $T = 10$ K also decrease at the beginning, then slightly increase and finally gradually decrease with increasing magnetic field. The first decrease in J_c is usually associated with weak pinning centers such as random disorder and point-like defects, in combination with strong single vortex pinning via or accompanied a change in the creep rate. When strong collective pinning sets in, J_c will increase to the SMP [25].

This increase in J_c is less pronounced for medium levels of C (0.03 and 0.07). At 10 K there is a more constant J_c region. This correlates to the shapes of the $M(T)$ curves in figure 2(a), and might be related to differences in sample homogeneity. Owing to the absence of a considerable density of strong pinning centers, the minimum in J_c at around 1 T is most pronounced for the undoped sample at elevated temperatures. Figure 4(d) compares J_c for the different samples at 5 T. With increasing C content, J_c first decreases then increases remarkably, where the minimum J_c with respect to the doping level seems to depend on temperature. At near zero field, the magnetically determined J_c of the 0.1 C sample is 1.33 times that of the undoped sample.

For either low T_c or high T_c a number of works have attempted to discover the origin of the peak effect in the magnetization. Depending on the particular system investigated, the origin has been found to have an association with different processes [25–29]. In order to shed light on the pinning mechanisms in the field region of the SMP in our samples, we studied the magnetic field dependence of the pinning force density F_p. $f_p = F_p/F_{p,max}$ is plotted as a function of reduced field $h = H/H_{max}$ instead of H/H_{irr} (as is usual for high-temperature superconductors) [30, 31] in figure 5(a), where $F_{p,max} = F_p(H = H_{max})$ is the maximum of F_p. This allows us to analyze the pinning mechanism even though J_c could not

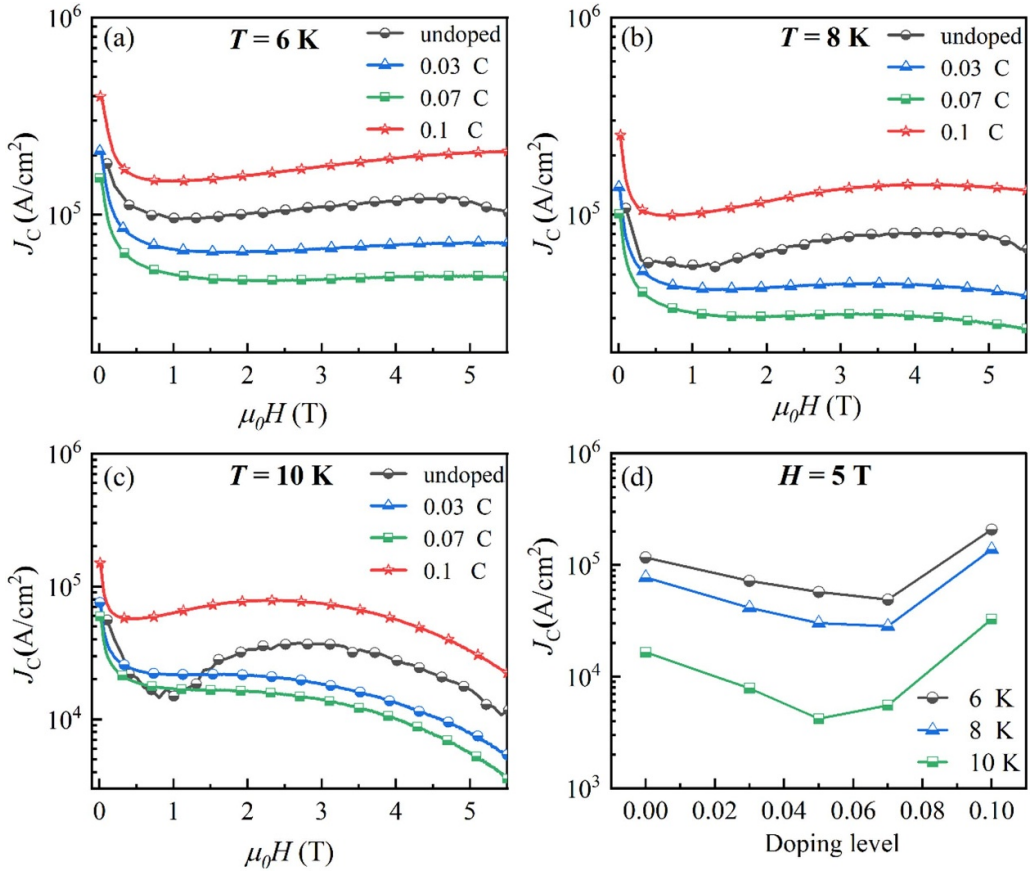

Figure 4. Magnetic field dependence of the critical current density (J_c) at different temperatures and $H//c$ in all samples measured at (a) 6 K, (b) 8 K and (c) 10 K. (d) J_c of all samples at 5 T with different amounts of C doping.

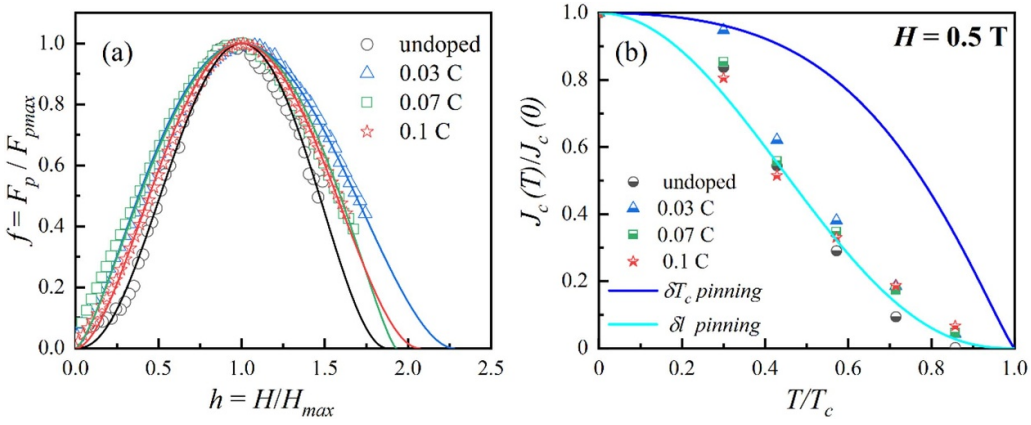

Figure 5. (a) Normalized pinning force density: plot of the normalized pinning force $f = F_p/F_{pmax}$ versus $h^* = H/H_{max}$. (b) Normalized J_c versus T/T_c for all the samples with different C contents.

be measured up to H_{irr}. Theoretically, f_p is described by the following formula:

$$f_p = \left(\frac{p}{q}\right)^q h^p \left(\frac{p+q}{p} - h\right)^q \quad (2)$$

where p and q are two parameters depending on the pinning mechanism. This is analogous to the Dew-Hughes formula [32]. The values of the fit parameter for all samples at 10 K are shown in table 1.

The irreversibility field can now be estimated from $H_{irr} = (p+q)/pH_{max}$ [33, 34]. Generalizing the Dew-Hughes

Table 1. Parameters p and q for the fits of $F_p(H)$ according to equation (2) for the different samples at 10 K as well as H_{irr} and h_{max}.

Sample	p	q	H_{irr} (T)	$h_{max} = H_{max}/H_{irr}$
Undoped	2.44	2.00	6.771	0.55
0.03 C	1.50	1.89	7.392	0.45
0.07 C	1.55	1.45	6.596	0.52
0.1 C	1.91	2.23	7.595	0.46

analysis, $h_{max} = p/(p + q)$ can be used to determine the predominant pinning mechanism [32, 35]. As shown by Yamamoto *et al* [36], $h_{max} \approx 0.45$ for $BaFe_{1.8}Co_{0.2}As_2$ suggests a possible correlation with a uniform Co distribution. Sun *et al* [37] did a similar analysis for a number of electron-doped and hole-doped Fe-arsenide superconductors, which included $Ba_{0.68}K_{0.32}Fe_2As_2$ ($h_{max} \approx 0.43$). Similar dopant-dependent variations in h_{max} have been observed in the isovalently doped 122 material $BaFe_2(As_{1-x}P_x)_2$ ($h_{max} = 0.35$–0.7) [38]. Dew-Hughes points out six pinning types: $p = 1, q = 2$ ($h_{max} = 0.33$) for normal core pinning; $p = 0.5$, $q = 2$ ($h_{max} = 0.2$) for normal surface pinning; $p = 0$, $q = 2$ ($h_{max} = 0$) for normal volume pinning; $p = 2$, $q = 1$ ($h_{max} = 0.67$) for $\delta\kappa$ point pinning; $p = 1.5$, $q = 1$ ($h_{max} = 0.6$) for $\delta\kappa$ surface pinning; and $p = 1$, $q = 1$ ($h_{max} = 0.5$) for $\delta\kappa$ volume pinning [39, 40]. In our case, all samples show $h_{max} \sim 0.50$, i.e. $\delta\kappa$ volume pinning, with the 0.03 C and 0.1 C samples showing a somewhat lower value, i.e. a possible contribution of normal point pinning.

To obtain further insight into the effect of C doping on the pinning mechanism in $FeSe_{0.5}Te_{0.5}$, the experimental results were analyzed using the theory of collective pinning at weak pinning centers [41]. This is reasonable for single crystals since strong pinning centers should be sparse. Also here, there are two principal mechanisms: δl pinning, due to spatial variations in the charge carrier mean free path, and δT_c pinning that comes from randomly distributed spatial variations in T_c. According to the theoretical approach proposed by Griessen *et al* [41], this is described by the following formulae [20]:

for δl pinning

$$J_c(t)/J_c(0) = \left(1 - t^2\right)^{5/2}\left(1 + t^2\right)^{-1/2} \quad (3)$$

and for δT_c pinning

$$J_c(t)/J_c(0) = \left(1 - t^2\right)^{7/6}\left(1 + t^2\right)^{5/6} \quad (4)$$

where $t = T/T_c$. Figure 5(b) compares the experimental J_c values at 0.5 T of samples with different C doping contents with these predictions. The experimental results and the δl pinning theoretical curve agree very well for all samples, confirming that pinning in the C-doped samples also originates from spatial variations of the mean free path and that weak point-like pinning centers play a dominant role [42]. From observations of figure 5(b), the δl pinning mechanism is the domain factor in all samples, suggesting the occurrence of vortex pinning by randomly distributed weak pinning centers [43]. Carbon doping may not cause obvious changes the pinning mechanism in the $FeSe_{0.5}Te_{0.5}$ samples.

The temperature dependence of electrical resistivity, $\rho(T)$, under applied magnetic fields of 0–9 T was measured for all samples as shown in figures 6(a)–(d). T_c gradually shifts toward lower temperatures as the field increases at a rate of 0.25 K T^{-1} for 0.1 C, 0.23 K T^{-1} for 0.07 C, 0.20 K T^{-1} for 0.03 C and 0.19 K T^{-1} for the undoped sample at 9 T. This indicates that the C doping process has hardly any influence on the critical damping temperature.

The Ginzburg–Landau coherence length $\xi(0)$ is obtained from $H_{c2}(0) = \Phi_o/2\pi\xi(0)^2$. In this formulation $\Phi_o = 2.0678 \times 10^{-15}$ Tm^2 represents the flux quantum and the 90% criterion for H_{c2} was used. The $\xi(0)$ values are shown in table 2. The increase in $H_{c2}(0)$ and corresponding smaller $\xi(0)$ values with C doping imply that electrical properties can be controllably tuned through introduction of C.

Basically, for the practical manufacture of superconducting magnets and wires, the behavior of H_{irr} together with the temperature dependence of the upper critical field H_{c2} as significant parameters should be taken into consideration [44, 45]. Vortices are able to move freely without any shackles and pinning is zero. In figure 6(e), H_{irr} and $H_{c2}(0)$ for all samples have been fitted with the equation $H(T/T_c) = H(0)^*(1 - T/T^*)^n$ [46, 47] as described in some papers, which is a function of temperature, where T^* is the zero-resistance temperature in zero field. All the critical information we can fit from the data is shown in table 2. These parameters are similar to literature data for the IBS 11 family [48–50] and correspond to the predicted value of 4/3 for a glass–liquid transition within error bars. The $H_{irr}(0)$ value for the 0.1 C sample is almost 1.05 times higher than for the undoped sample. In table 2, $H_{c2}(0)$ is larger than $H_{irr}(0)$ for all samples. The more C that is introduced in the system, the higher $H_{c2}(0)$ and $H_{irr}(0)$ and the smaller $\xi(0)$. This suggests that C doping could control the intrinsic electrical properties and thus tune and improve the superconductivity.

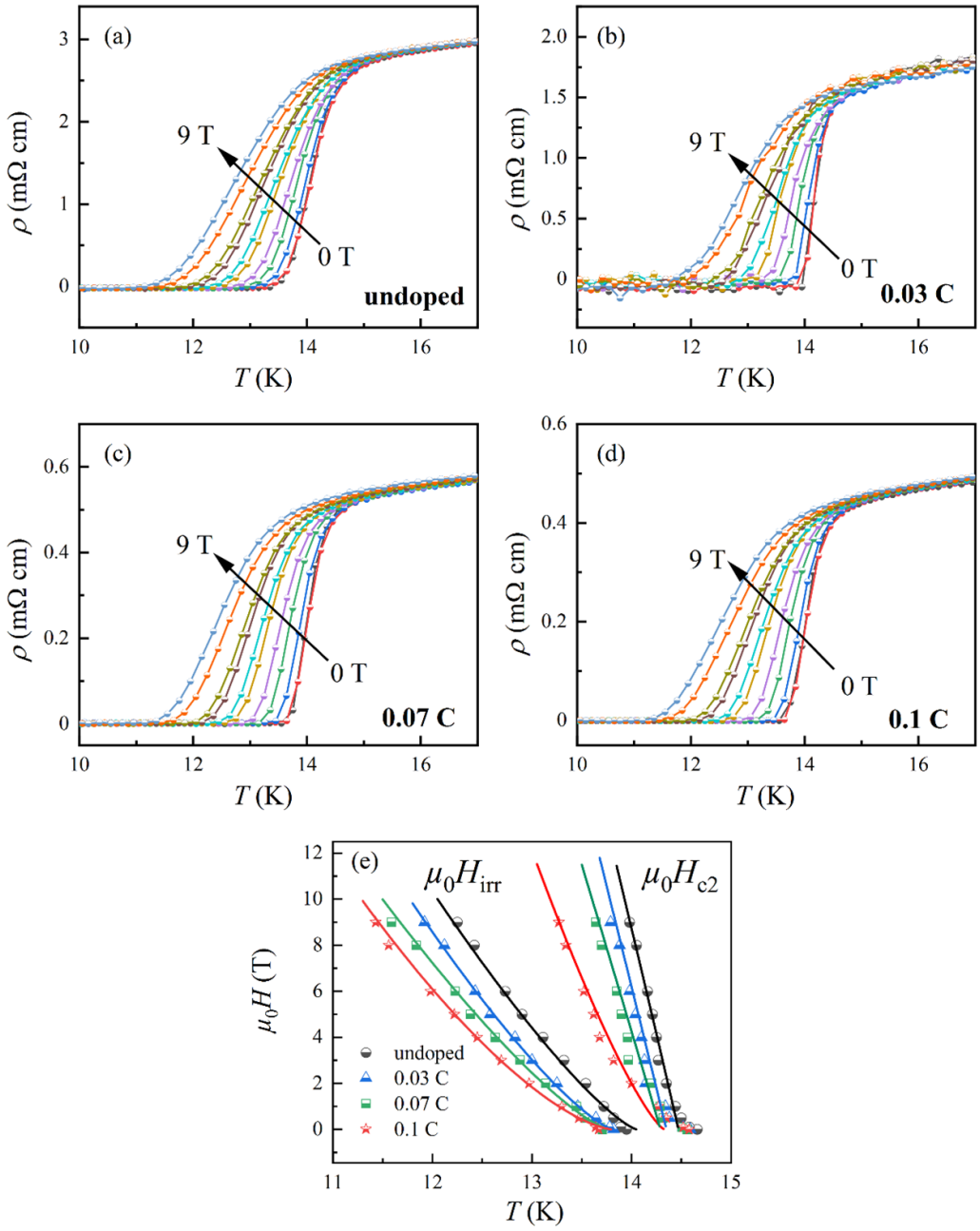

Figure 6. (a)–(d) Resistivity $\rho(T)$ as a function of temperature for different magnetic fields and (e) the upper critical (H_{c2}) and irreversibility (H_{irr}) fields estimated for samples with different C doping contents.

Table 2. Estimates for the orbital upper critical field at 0 K for three criteria (see text) in dependence on C doping.

C content x	$H_{c2}(0)$ at 90% ρ_n(T)	$H_{irr}(0)$ (T)	$\xi(0)$ (Å)	n_{irr}	n_{Hc2}
0	251	119	11.45	1.27	0.98
0.03	245	120	11.59	1.30	0.99
0.07	202	104	12.76	1.30	0.99
0.1	260	126	11.25	1.49	1.29

4. Conclusions

We have successfully prepared C-doped $FeSe_{0.5}Te_{0.5}$ single crystals for the first time and investigated their structural and superconducting properties by magnetization and electrical transport measurements. Carbon doping of the $FeSe_{0.5}Te_{0.5}$ system does not change the tetragonal P4/*nmm* crystal structure and leads to a slight decrease in T_c. The expansion of the unit cell indicates incorporation of C into the $FeSe_{0.5}Te_{0.5}$ crystal structure. We find large J_c as well as a second peak effect in the undoped and the 0.1 C samples. Furthermore, C doping changed the intrinsic superconducting properties, pointing to the dominance of the δl pinning mechanism in all the samples and suggesting the occurrence of vortex pinning by randomly distributed weak pinning centers. According to the resistivity data, the introduction of C increases J_c, $H_{irr}(0)$ and $H_{c2}(0)$. The introduction of C provides a platform for improving J_c and $H_{c2}(0)$ in $FeSe_{0.5}Te_{0.5}$ samples.

Data availability statement

The data that support the findings of this study are available upon reasonable request from the authors.

Acknowledgments

The research was supported by the Sichuan Applied Basic Research Project (Grant No. 2018JY0003). We would like to thank Analytical and Testing Center of Southwest Jiaotong University.

ORCID iDs

Jens Hänisch https://orcid.org/0000-0003-2757-236X
X S Yang https://orcid.org/0000-0002-8686-9860
K Zhao https://orcid.org/0000-0002-9296-6253
Y Zhao https://orcid.org/0000-0002-8774-3629

References

[1] Bartlett J, Steppke A, Hosoi S, Noad H and Hicks C W 2021 *Phys. Rev.* X **11** 021038
[2] Yao C and Ma Y 2021 *iScience* **24** 102541
[3] Faeth B D, Yang S, Kawasaki J K, Nelson J N, Mishra P, Chen L, Schlom D G and Shen K M 2021 *Phys. Rev.* X **11** 021054
[4] Kurokawa H, Nakamura S, Zhao J, Shikama N, Sakishita Y, Sun Y, Nabeshima F, Imai Y, Kitano H and Maeda A 2021 *Phys. Rev.* B **104** 014505
[5] Sales B C, Sefat A S, Mcguire M A, Jin R Y, Mandrus D and Mozharivskyj Y 2009 *Phys. Rev.* B **79** 094521
[6] Patel U, Hua J, Yu S H, Avci S and Kwok W K 2009 *Appl. Phys. Lett.* **94** 082508
[7] Fernandes R M, Coldea A I, Ding H, Fisher I R, Hirschfeld P J and Kotliar G 2022 *Nature* **601** 35–44
[8] Li Y, Zaki N and Garlea V O 2021 *Nat. Mater.* **20** 1221–7
[9] Kumar S and Singh P P 2016 *J. Alloys Compd.* **663** 295–310
[10] Maheshwari P K, Gahtori B, Gupta A and Awana V 2017 *AIP Adv.* **7** 015006
[11] Zhang A M, Xia T L, Kong L R, Xiao J H and Zhang Q M 2010 *J. Phys.: Condens. Matter* **22** 245701
[12] Sala A, Palenzona A, Bernini C, Caglieris F and Putti M 2013 *Physica* C **494** 69–73
[13] Thakur G S, Haque Z, Neha P, Gupta L C and Ganguli A K 2014 *Z. Anorg. Allg. Chem.* **640** 1159–63
[14] Galluzzi A, Polichetti M, Buchkov K, Nazarova E, Mancusi D and Pace S 2016 *Supercond. Sci. Technol.* **30** 025013
[15] Bhagurkar A G, Yamamoto A, Wang L, Xia M, Dennis A R, Durrell J H, Aljohani T A, Babu N H and Cardwell D A 2018 *Sci. Rep.* **8** 13320
[16] Gong C, Zhao Q, Ping X, Zhang P and Hao L 2020 *J. Mater. Sci., Mater. Electron.* **31** 15336–44
[17] Yadav A K, Thakur A D and Tomy C V 2013 *Phys. Proc.* **49** 109–17
[18] Shipra R, Takeya H, Hirata K and Sundaresan A 2010 *Physica* C **470** 528–32
[19] Klein L, Yacoby E R, Yeshurun Y, Erb A, Müller-Vogt G, Breit V and Wühl H 1994 *Phys. Rev.* B **49** 4403
[20] Bonura M, Giannini E, Viennois R and Senatore C 2012 *Phys. Rev.* B **85** 134532
[21] Galluzzi A, Buchkov K, Tomov V, Nazarova E, Leo A, Grimaldi G, Nigro A, Pace S and Polichetti M 2018 *Supercond. Sci. Technol.* **31** 015014
[22] Prozorov R, Ni N, Tanatar M A, Kogan V G and Canfield P C 2008 *Phys. Rev.* B **78** 224506
[23] Yang H, Luo H, Wang Z and Wen H H 2008 *Appl. Phys. Lett.* **93** 142506
[24] Bean C P 1962 *Phys. Rev. Lett.* **8** 250–3
[25] Polichetti M, Galluzzi A, Buchkov K, Tomov V, Nazarova E, Leo A, Grimaldi G and Pace S 2021 *Sci. Rep.* **11** 7247
[26] Kováč P, Hugek I and Meligk T 2004 *Supercond. Sci. Technol.* **17** 1225
[27] Yu Z, Banno N, Zhao Y and Tachikawa K 2019 *Supercond. Sci. Technol.* **32** 035003
[28] Krusin-Elbaum L, Civale L, Vinokur V M and Holtzberg F 1992 *Phys. Rev. Lett.* **69** 2280
[29] Rosenstein B and Knigavko A 1999 *Phys. Rev. Lett.* **83** 844
[30] Iida K, Cayado P, Rijckaert H, Erbe M, Hänisch J, Okada T, Driessche V I, Awaji S and Holzapfel B 2021 *Supercond. Sci. Technol.* **34** 015009
[31] Liu J *et al* 2022 *ACS Appl. Mater. Interfaces* **14** 2246
[32] Dew-Hughes D 1974 *Phil. Mag.* **30** 293–305
[33] Higuchi T, Yoo S I and Murakami M 1999 *Phys. Rev.* B **59** 1514
[34] Hänisch J, Iida K and Cayado P 2022 *Supercond. Sci. Technol.* **35** 084009
[35] Campbell A M, Evetts J E and Dew-Hughes D 1968 *Phil. Mag.* **18** 313–43
[36] Yamamoto A *et al* 2009 *Appl. Phys. Lett.* **94** 062511
[37] Sun D L, Liu Y and Lin C T 2009 *Phys. Rev.* B **80** 144515
[38] Fang L, Jia Y, Schlueter J A, Kayani A, Xiao Z L, Claus H, Welp U, Koshelev A E, Crabtree G W and Kwok W-K 2011 *Phys. Rev.* B **84** 140504
[39] Wu Z, Wang Z, Tao J, Qiu L, Yang S and Wen H 2016 *Supercond. Sci. Technol.* **29** 035006
[40] Zhao J and Wang Z 2022 *J. Alloys Compd.* **917** 165358
[41] Griessen R, Wen H H, Van Dalen A J, Dam B and Bruynseraede Y 1994 *Phys. Rev. Lett.* **72** 1910–3
[42] Wang C, He T, Chen D, Zhang J, Fan C, Tang Q, Dong C, Tu Y, Yu B and Ma Y 2021 *Supercond. Sci. Technol.* **34** 115020

[43] Wang C, He T, Han Q, Fan C, Tang Q, Chen D, Lei Q, Sun S, Li Y and Yu B 2021 *Supercond. Sci. Technol.* **34** 055001
[44] Ma Y 2012 *Supercond. Sci. Technol.* **25** 113001
[45] Tanabe K and Hosono H 2012 *Jpn. J. Appl. Phys.* **51** 010005
[46] Shen B, Cheng P, Wang Z, Fang L, Ren C, Shan L and Wen H H 2010 *Phys. Rev.* B **81** 014503
[47] Shahbazi M, Wang X L, Choi K Y and Dou S X 2013 *Appl. Phys. Lett.* **103** 032605
[48] Hosono H, Yamamoto A, Hiramatsu H and Ma Y 2018 *Mater. Today* **21** 278–302
[49] Leo A *et al* 2017 *IEEE Trans. Appl. Supercond.* **27** 7300405
[50] Galluzzi A, Buchkov K, Nazarova E, Tomov V, Grimaldi G, Leo A, Pace S and Polichetti M 2019 *Eur. Phys. J* **228** 725